Electrochemical oxidation of hydrogen peroxide at platinum electrodes. Part 1: An adsorption controlled mechanism. Electrochim Acta

ARTICLE *in* ELECTROCHIMICA ACTA · NOVEMBER 1997

Impact Factor: 4.5 · DOI: 10.1016/S0013-4686(97)00125-4

3 AUTHORS, INCLUDING:

Emad A Khudaish
Sultan Qaboos University
17 PUBLICATIONS **284** CITATIONS

Pergamon

Electrochimica Acta, Vol. 43, Nos 5–6, pp. 579–588, 1998

Printed in Great Britain
PII: S0013-4686(97)00125-4
0013–4686/98 $19.00 + 0.00

Electrochemical oxidation of hydrogen peroxide at platinum electrodes. Part 1. An adsorption-controlled mechanism

Simon B. Hall,[a]* Emad A. Khudaish[a] and Alan L. Hart[b]

[a]Department of Chemistry, Massey University, Private Bag 11222, Palmerston North, New Zealand

[b]Sensor Group, AgResearch, Grasslands Research Centre, Palmerston North, New Zealand

(Received 21 October 1996; in revised form 14 February 1997)

Abstract—The electrochemical oxidation of H_2O_2 at a platinum rotating disk electrode was studied at pH 7.26 for the [H_2O_2] range 0–80 mM and for rotation rates 630–10,000 r.p.m. A mechanism is proposed to account for the steady-state current response as a function of both rotation rate and [H_2O_2]. The mechanism incorporates reversible binding of hydrogen peroxide to electrochemically generated Pt(II) surface sites with inhibiting competitive adsorption of dioxygen at these sites. A further inhibiting side reaction is also identified involving protonation of the surface adsorbed H_2O_2 complex. © 1997 Elsevier Science Ltd

Key words: platinum, hydrogen peroxide, oxidation, rotating disk electrode, mechanism.

INTRODUCTION

The use of platinum as a catalytic material for the electrochemical oxidation of hydrogen peroxide is widespread in the construction of amperometric biosensors. In these devices, hydrogen peroxide is generated in a preceding enzyme reaction so that the rate of subsequent electrochemical oxidation is linearly proportional to the analyte concentration [1]. A prime example is that of glucose sensors incorporating glucose oxidase (GOx). The reactions are:

$$\text{glucose} + O_2 \xrightarrow{\text{GOx}} \text{gluconic acid} + H_2O_2, \quad (1)$$

$$H_2O_2 \xrightarrow{\text{electrode}} O_2 + 2H^+ + 2e^-. \quad (2)$$

Many devices incorporate the platinum (or other metals such as palladium or rhodium) as fine dispersions on carbon [2, 3]. Here, highly catalytic surfaces are achieved so long as the particle size of the dispersed metal is comparable to that of the electric double layer [4]. Furthermore, the use of metallized carbon permits the mass-production of high surface area electrodes by screen-printing [5, 6].

One limiting parameter for the linear range of biosensors is the potential for the enzyme to exhibit analyte-independent response due to substrate saturation. The concentration at which this becomes significant is determined by the K_M value for the enzyme. Addition of an outer polymer membrane or dispersion of the enzyme within a membrane acts to decrease this problem [7].

Reaction (2) also exhibits deviations from linearity which may impact upon the overall response of sensors. Zhang and Wilson [8] examined the oxidation of H_2O_2 on platinum and platinum/iridium wire electrodes and found that a pronounced depression of response is evident for hydrogen peroxide concentrations above 1 mM, both in steady state measurements and in extrapolated kinetic currents for a series of Koutecky–Levich plots [9]. These workers accounted for the deviation in terms of saturation of the electrode surface by H_2O_2 and O_2 based on earlier reports for potentiometric measurements [10]. They also suggested that slow electron transfer might impose kinetic control on the overall process so that the current is no longer proportional to the bulk H_2O_2 concentration.

A number of other factors influence the response of solid Pt electrodes. Most notably is that oxidation of H_2O_2 is favored on oxidized Pt surfaces [11–13].

*Author to whom correspondence should be addressed.

These findings were based on the potential at which H_2O_2 was observed to oxidize. This potential region had previously been shown to correspond to platinum oxide film formation [14]. Lingane and Lingane [12] supported the earlier suggestion by Hickling and Wilson [15] that the primary electron transfer reaction is the re-oxidation of platinum to platinum oxides, after the oxide film had previously been reduced by hydrogen peroxide.

It should be noted that there is a further complication as cathodic pre-treatment to remove adsorbed oxygen promotes the overall reaction [16].

A number of workers have explored the oxidation of H_2O_2 on thin palladium/gold layers. Gorton [17] found non-linear steady-state response to H_2O_2 above 10 mM for sputtered Pd/Au on carbon. Assuming that gold only acts to aid dispersion of palladium, they proposed that oxidation was reliant on surface oxide films in a similar manner to that found for Pt and follows the scheme:

$$Pd(OH)_2 + H_2O_2 \rightarrow Pd + 2H_2O + O_2 \qquad (3)$$

$$Pd + 2H_2O \rightarrow Pd(OH)_2 + 2e^- + 2H^+. \qquad (4)$$

Johnston *et al*. assembled Pd/Au thin-film electrodes by vacuum evaporation on PVC supports [18]. These workers observed similar results to those of Gorton and they explored the form of the deviation from linearity by consideration of a surface binding site model that incorporates reactions (3) and (4) above:

$$H_2O_{2\,bulk} \xrightarrow{\text{diffusion}} H_2O_2, \qquad (5)$$

$$H_2O_2 + Pd(OH)_2 \rightleftharpoons Pd(OH)_2{\cdot}H_2O_2, \qquad (6)$$

$$Pd(OH)_2{\cdot}H_2O_2 \rightarrow Pd + 2H_2O + O_2, \qquad (7)$$

$$Pd + 2H_2O \rightarrow Pd(OH)_2 + 2H^+ + 2e^-, \qquad (8)$$

where reaction (5) represents diffusion of hydrogen peroxide to the electrode surface. It is assumed that the surface complex is in rapid equilibrium and sufficiently anodic potentials are applied so that reaction (8) is more rapid than (7).

Johnston *et al*. demonstrated that for fixed cell geometry and stirring conditions (unspecified) double reciprocal plots (equivalent to Lineweaver–Burk plots) of 1/rate against $1/[H_2O_2]$ gave linear relationships. This is suggestive of the system obeying a form of Michaelis–Menten kinetics with the intercept of the Lineweaver–Burk plot indicating the maximum rate for the reaction at maximum occupancy of surface sites.

In this paper we extend the findings of Johnston *et al*. to the oxidation of H_2O_2 on a solid platinum rotating disk electrode over a range of concentrations and rotation rates so that the extent of diffusion control and nature of the surface kinetics can be evaluated.

EXPERIMENTAL

All chemicals used were from Univar and were of the highest purity available and all solutions were prepared in Millipore water. Hydrogen peroxide (30% w/w) was standardized by titration against acidified solutions of $KMnO_4$ which was prepared immediately prior to use and standardized against anhydrous disodium oxalate.

All electrochemical measurements were made in 250 cm^3 of a pH 7.26 phosphate buffer (0.1 M) in a specially designed water-jacketed cell maintained at $20 \pm 0.05^{\circ}C$ with a circulating water bath (Colora, Messtechnik GmbH, Germany) and monitored with a calibrated thermocouple placed within the cell at the same height as the working electrode. The electrolyte was degassed with stirring by purging with oxygen-free nitrogen for 15 min prior to immersion of the electrode and maintained throughout experimentation. Hydrogen peroxide was added to the electrolyte as a series of 100 μl aliquots of the standardized concentrated solution.

All electrodes and electrochemical equipment were from Bioanalytical Systems Inc. (BAS) Indiana, U.S.A. A platinum disc electrode with geometric area 0.1195 cm^2 was used as the working electrode, a Pt coil (area 1.9 cm^2) employed as the counter and an Ag/AgCl gel electrode (3 M NaCl) of potential +0.197 V vs *she* as the reference electrode. The working electrode was mounted (in an inverted orientation) in a BAS RDE-1 rotating disk electrode assembly connected to a BAS-100B electrochemical analyzer. Electrochemical experiments were programmed using the BAS-100B software.

The working electrode was conditioned prior to electrochemical measurements by cyclic voltammetry between the potential limits 0.0 V and +1.0 V vs Ag/AgCl at 100 mV s^{-1} for 50 cycles and terminating at the anodic potential limit on the final cycle.

Chronoamperometric measurements for the oxidation of H_2O_2 were made by stepping the potential of the working electrode from +200 mV to +600 mV vs Ag/AgCl. This potential was selected for maximum oxidation rate of H_2O_2 and is consistent with previously reported values [19] and values commonly employed in biosensors [3, 20, 21]. The anodic potential was held for 20 s by which time the current had adopted a steady-state value. The last second of digitized data (50 points) was averaged for each experiment and the mean value and standard deviation recorded. In all cases reported here, the maximum standard deviation was 5×10^{-5} mA cm^{-2} and, thus, deviations are too small to include as error bars in the figures.

Chronoamperometric measurements were made over the H_2O_2 concentration range 0–80 mM and for rotation rates, ω, of 630, 1000, 1585, 2500, 4000, 6300 and 10,000 r.p.m. These rotation rates were selected so that they were evenly spaced in $\omega^{-1/2}$.

The problem of O_2 bubbles diminishing the area of the inverted electrode exposed to the electrolyte was avoided by rapidly increasing the rotation rate of the *rde* to the maximum rate possible (10,000 r.p.m.) immediately prior to the potential step sequence by application of an external analog signal to the BAS RDE-1.

The average response and standard deviation for each chronoamperometric experiment was calculated and collated using software developed during the course of this work. The constants for the model were optimized using a Simplex [22–25] algorithm encoded in purpose-written software [26] and results displayed with Microsoft Excel (5.0). All software developed during the course of this work was compiled using Borland Turbo Pascal (7.0).

RESULTS AND DISCUSSION

The steady-state response of a Pt rotating disk electrode to H_2O_2 for a range of bulk concentrations and rotation rates is shown in Fig. 1. It should be noted that the data was collected for a single series of experiments with no electrode conditioning (either physical or electrochemical) between successive concentrations or rotation rates. Previous workers have shown that oxidation of H_2O_2 on Pt is dependent on the oxidation of the surface [11–13], the primary electron transfer being the re-oxidation of Pt formed as a consequence of reduction by H_2O_2 [12, 15]. Our experimental conditions involve establishing a reproducible electrode surface by cyclic voltammetry in the potential region in which surface oxides will form [14]. All subsequent chronoamperometric measurements involve stepping from a potential close to the open circuit value to the anodic region for a sufficient time so that steady-state conditions are achieved. This approach minimises the extent to which the number of surface sites will change during successive additions of H_2O_2.

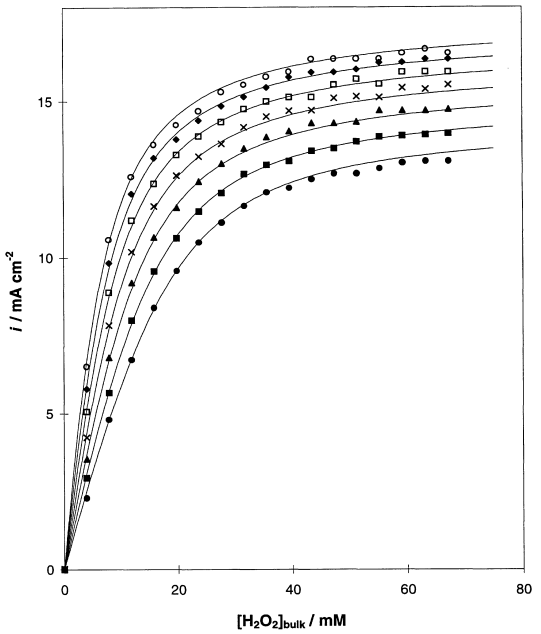

Fig. 1. Steady-state current responses ($E = +600$ mV vs Ag/AgCl) as a function of bulk hydrogen peroxide for a range of rotation rates. ● 630 r.p.m., ■ 1000 r.p.m., ▲ 1585 r.p.m., × 2500 r.p.m., □ 4000 r.p.m., ◆ 6300 r.p.m. and ○ 10,000 r.p.m. Smooth curves are the synthetic responses calculated using the model and parameters developed in this paper.

At each rotation rate the current exhibits linear dependence on $[H_2O_2]$ in the range 0–10 mM. The current response increases from 0.60 mA cm^{-2} mM^{-1} at 630 r.p.m. to 1.75 mA cm^{-2} mM^{-1} at 10,000 r.p.m. indicating that the process involves diffusion. The linear dependence is progressively curtailed so that for $[H_2O_2] > 50$ mM a limiting current is approached at all rotation rates with the limiting current being greater for higher rotation rates.

Koutecky–Levich study

Previous workers [8] have analyzed the oxidation of H_2O_2 using Koutecky–Levich plots [9] where the electrode reaction is treated as an irreversible process involving both kinetic and mass transfer components. The general relationship for such a process is given by

$$\frac{1}{i} = \frac{1}{i_k} + \frac{1}{i_d}. \tag{9}$$

The kinetic current, i_k, is given by

$$i_k = nFk_f[H_2O_2]_{bulk}, \tag{10}$$

where k_f is the heterogeneous electron transfer rate constant and $[H_2O_2]_{bulk}$ is the bulk concentration in mol m^{-3} (or mM). The diffusion current, i_d, given by

$$i_d = 0.620nF[H_2O_2]_{bulk}\ D_{H_2O_2}^{2/3}\ v^{-1/6}\ \omega^{1/2}, \tag{11}$$

where $D_{H_2O_2}$ is the diffusion coefficient, v is the kinematic viscosity (taken to be 1.00×10^{-6} m^2 s^{-1}) and ω is in rad s^{-1}. Thus, for kinetic and mass transfer controlled reactions a Koutecky–Levich plot of $1/i$ vs $1/\omega^{1/2}$ for each concentration should result in linear relationships from which the kinetic current and diffusion coefficient may be evaluated. Figure 2 displays the Koutecky–Levich plot for the experimental data shown in Fig. 1 in the concentration range 0–30 mM (data above this are omitted for clarity). Predominantly linear relationships are observed with slope decreasing with increasing $[H_2O_2]$ in agreement with that observed by Zhang and Wilson [8]. Linear regression analysis shows the Koutecky–Levich plots have similar intercepts with the $1/i$ axes with i_k having values ranging from 17.3 to 19.2 mA cm^{-2}. This is in marked contrast to that found by Zhang and Wilson [8] where the intercept was dependent on concentration and i_k was found to be linearly dependent on $[H_2O_2]$ at low concentration. These workers noted departure from linearity above 1 mM and

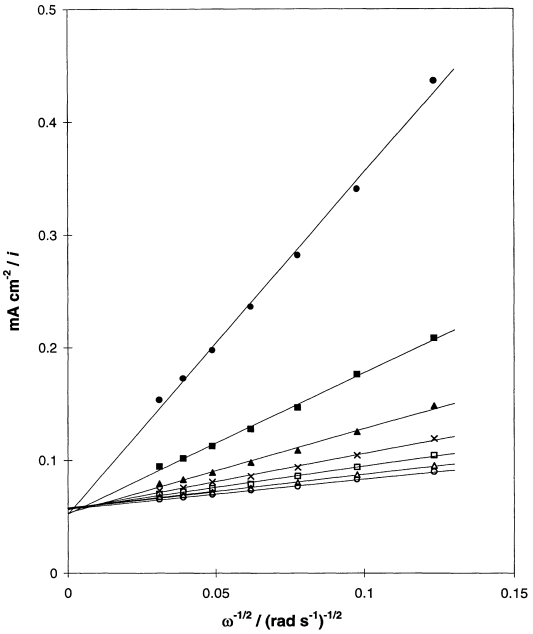

Fig. 2. Koutecky–Levich plots of the data presented in Fig. 1 for a selection of bulk hydrogen peroxide concentrations (higher concentrations omitted for clarity). ● 4.0 mM, ■ 8.0 mM, ▲ 11.9 mM, × 15.9 mM, □ 19.9 mM, △ 23.8 mM and ○ 27.8 mM.

ascribed this decrease in response to saturation of the electrode surface by H_2O_2 and O_2. We suggest here that whilst i_k increases at low concentrations it proceeds to adopt a constant value at the higher concentrations explored in this work.

Close inspection of Fig. 2 reveals that the plots display progressively more parabolic departures from linearity with increasing $[H_2O_2]$. This indicates that Koutecky–Levich analysis is not sufficient to completely describe this electrode reaction.

Diffusion coefficients for H_2O_2 were evaluated using equation (11) and the slopes of the linear relationships shown in Fig. 2 (together with those not plotted for reasons of clarity). This parameter should be invariant with concentration. Inspection of the plots of $D_{H_2O_2}$ as a function of $[H_2O_2]$ in Fig. 3 shows, however, that the apparent diffusion coefficient varies greatly and exhibits values of *ca.* $0.6 \times 10^{-9}\,m^2\,s^{-1}$ at both extremes of the concentration range explored and a maximum of $1.4 \times 10^{-9}\,m^2\,s^{-1}$ at 30 mM. Previous workers have used the hydrodynamic response for the oxidation of H_2O_2 at Pt to determine the diffusion coefficient for this species. Recently van Stroe-Biezen *et al.* [27] reported a value of $1.43 \times 10^{-9}\,m^2\,s^{-1}$ at 25°C and at an unspecified H_2O_2 concentration. Whilst this value is similar to those found by Prabhu *et al.* [19] for the reduction of H_2O_2 by chronoamperometric and chronopotentiometric techniques in quiescent solutions and also that found by Borggaard [28] using polarography, we suggest that use of this value is treated with caution in light of our findings.

The results shown in Figs 2 and 3 strongly suggest that it is likely that the oxidation of H_2O_2 at Pt proceeds by a mechanism somewhat more complicated than electron transfer coupled with diffusion control. Accordingly, in the following section we assess the applicability of the Michaelis–Menten kinetic analysis employed by Johnston *et al.* [18] for the oxidation of H_2O_2 at Pd/Au thin-films to our system.

Michaelis–Menten study

We have analyzed our experimental results in terms of Michaelis–Menten kinetics using the Hanes plot method [29] in preference to the Lineweaver–Burk approach [30] since the latter method suffers from undue weighting on low concentration data. The general form of the Hanes plot for Michaelis–Menten kinetics is given by

$$\frac{[H_2O_2]}{j} = \left(\frac{1}{j_{max}}\right)[H_2O_2] + \frac{K_M}{j_{max}}, \qquad (12)$$

where j is the rate (in mol $m^{-2}\,s^{-1}$) given by

$$j = \frac{i}{nF}, \qquad (13)$$

j_{max} is the maximum rate under saturation conditions and K_M is the Michaelis constant.

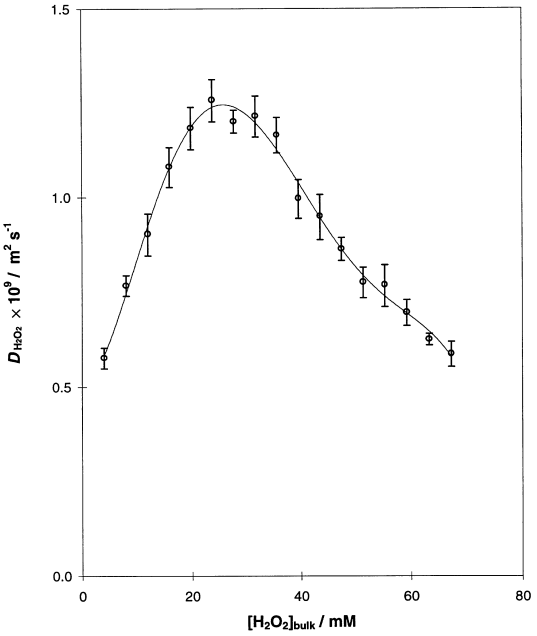

Fig. 3. Diffusion coefficients for H_2O_2 as a function of bulk concentration calculated using equation (11) from the slopes of the Koutecky–Levich plots presented in Fig. 2 (including data omitted for clarity). The error bars were calculated from the estimated error in the Koutecky–Levich slopes.

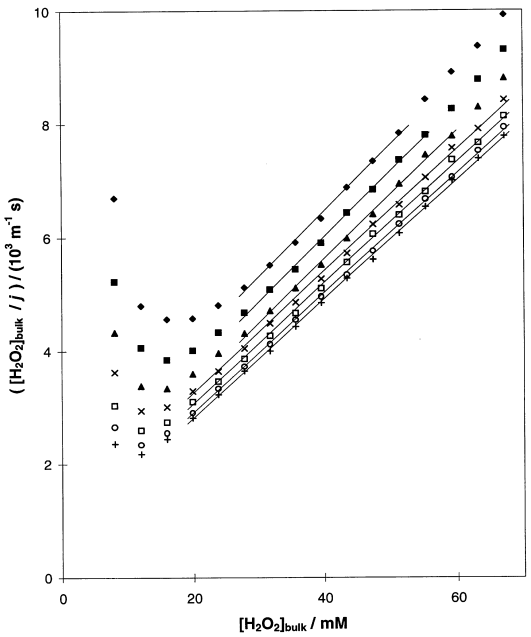

Fig. 4. Hanes plots for the data presented in Fig. 1. Regions selected for determination of $K_{M\,app}$ and j_{max} are indicated by solid lines. ◆ 630 r.p.m., ■ 1000 r.p.m., ▲ 1585 r.p.m., × 2500 r.p.m., □ 4000 r.p.m., ○ 6300 r.p.m. and + 10,000 r.p.m.

The Hanes plots for the steady-state data in Fig. 1 is shown in Fig. 4. It is apparent that Michaelis–Menten kinetics is only approached at all concentrations for the highest rotation rates explored with pronounced deviations evident at lower rotation rates in the concentration region 0–15 mM. Linear regions may be identified at all rotation rates at higher concentrations indicating that Michaelis–Menten kinetics have some role in the overall kinetics (although some deviation is also observed at high concentrations for low rotation rates). Table 1 lists apparent Michaelis constants ($K_{M\,app}$) and j_{max} values (together with the maximum current, i_{max} calculated using equation (13)) at each rotation rate for the linear regions identified by the solid lines in Fig. 4. The maximum rates and Michaelis constants are found to be consistent with estimated values obtainable from the data in Fig. 1 indicating that appropriate linear regions have been selected and is consistent with some form of Michaelis–Menten kinetics operating.

A decrease in $K_{M\,app}$ with increase in rotation rate might have been predicted for a reaction where some element of diffusion control is exhibited. Here, forced transport by electrode rotation would act to replenish the depletion of H_2O_2 at the electrode surface afforded by the reaction

$$H_2O_2 \xrightarrow{\text{electrode}} O_2 + 2H^+ + 2e^-. \qquad (2)$$

In this way, the bulk concentration required for half-saturation of the electrode would decrease with increased rotation rate. If this were the only effect of rotation, then the series of Hanes plots would exhibit linear responses with common slope and successively lower intercepts with increasing rotation rate. Instead, deviations from linearity are observed at low rotation rates and low concentrations indicating that another process operates in this region to decrease the rate of reaction from that expected.

A further unexpected result is evident in the data tabulated in Table 1 and displayed in Fig. 1 in that if rotation were only to aid transport of H_2O_2 to the electrode, then variation of j_{max} would not be observed. Instead, j_{max} is found to increase with rotation rate. Furthermore, our earlier Koutecky–Levich analyses indicates that there is dependence of j_{max} on $\omega^{-1/2}$ indicating the possibility of some diffusion control.

We propose that these results may be interpreted in terms of a mechanism involving Michaelis–Menten kinetics where the deviations in the Hanes plots at low concentrations and low rotation rates is due to a transient inhibition of the binding site by a reaction product and that another form of inhibition prevails at all concentrations as indicated by a variation in j_{max}.

The inhibition involves the reaction products since increasing the rotation rate increases the rate through forced removal of these species. Coupled with these effects is enhanced reaction rate with delivery of the reactant to the binding site as shown by a decrease in $K_{M\,app}$ with rotation rate in Table 1. In the following section we propose a modified form of Michaelis–Menten kinetics incorporating these features and optimize the surface equilibrium and heterogeneous rate constants for our experimental data.

Table 1.
Kinetic parameters for simple Michaelis–Menten kinetics calculated from the selected linear regions identified in Fig. 4

	ω/r.p.m.						
	630	1000	1585	2500	4000	6300	10,000
$K_{M\,app}$ (mol m^{-3})	15.8	12.3	9.9	10.4	8.8	7.6	6.8
$j_{max} \times 10^3$ (mol m^{-2} s^{-1})	0.863	0.871	0.886	0.932	0.938	0.948	0.954
i_{max} (mA cm^{-2})	16.7	16.8	17.1	18.0	18.1	18.3	18.4

A product-inhibited Michaelis–Menten mechanism

The results shown in Fig. 1 were analyzed according to the mechanistic scheme outlined below, whereby H_2O_2 is adsorbed onto Pt(II) binding sites according to a Langmuir isotherm. We have chosen to identify the Pt(II) binding site as $Pt(OH)_2$ to maintain consistency with the work of Johnston *et al*. [18] on Pd/Au films.

$$H_2O_2 + Pt(OH)_2 \overset{K_1}{\rightleftharpoons} Pt(OH)_2{\cdot}H_2O_2 \qquad (14)$$

where the adsorption constant K_1 is given by

$$K_1 = \frac{\theta_{Pt(OH)_2\cdot H_2O_2}}{[H_2O_2]\,\theta_{Pt(OH)_2}}, \qquad (15)$$

where θ_i refers to the fractional surface coverage of each species i in this and following expressions. In this and following expressions concentrations of species are those at the surface of the electrode unless otherwise stated.

Following adsorption the complex undergoes internal electron transfer with the formation of a zero oxidation state Pt site and the release of the products H_2O and O_2

$$Pt(OH)_2{\cdot}H_2O_2 \xrightarrow{k_2} Pt + 2H_2O + O_2. \qquad (16)$$

The binding site is regenerated electrochemically, giving rise to the observed current

$$Pt + 2H_2O \xrightarrow{k_3} Pt(OH)_2 + 2H^+ + 2e^-. \qquad (17)$$

Two inhibiting side reactions are identified in this mechanism. The first involves competitive binding of the reaction product O_2 to the Pt(II) binding site so that reaction (14) is blocked,

$$Pt(OH)_2 + O_2 \overset{K_4}{\rightleftharpoons} Pt(OH)_2{\cdot}O_2 \qquad (18)$$

where the competitive inhibition binding constant K_4 is given by

$$K_4 = \frac{\theta_{Pt(OH)_2\cdot O_2}}{[O_2]\,\theta_{Pt(OH)_2}}. \qquad (19)$$

The second involves reversible protonation of the surface $Pt(II)/H_2O_2$ complex where the protons are the product of reaction (17)

$$Pt(OH)_2{\cdot}H_2O_2 + H^+ \overset{K_5}{\rightleftharpoons} Pt(OH)_2{\cdot}H_2O_2{\cdot}H^+ \qquad (20)$$

The protonation constant K_5 is given by

$$K_5 = \frac{\theta_{Pt(OH)_2\cdot H_2O_2\cdot H^+}}{[H^+]\,\theta_{Pt(OH)_2\cdot H_2O_2}}. \qquad (21)$$

A sufficiently anodic potential is employed in the experiments reported here so that reaction (17) is not rate limiting and $\theta_{Pt}\rightarrow 0$. Thus, the steady-state rate, j, is given by the rate at which the surface $Pt(II)/H_2O_2$ complex undergoes internal electron transfer

$$j = k_2 N \theta_{Pt(OH)_2\cdot H_2O_2} \qquad (22)$$

where N is the number of binding sites per m^2.

Given that $\theta_{Pt}\rightarrow 0$, the fractional surface coverage balance equation is described by

$$1 = \theta_{Pt(OH)_2} + \theta_{Pt(OH)_2\cdot H_2O_2} + \theta_{Pt(OH)_2\cdot O_2} + \theta_{Pt(OH)_2\cdot H_2O_2\cdot H^+}. \qquad (23)$$

Applying the steady-state approximation to the adsorbed species, substitution of equations (14)–(16) and (18)–(22) into equation (23) and solving for j yields the product-inhibited Michaelis–Menten rate equation

$$j = \frac{k_2 N K_1 [H_2O_2]}{1 + K_4[O_2] + K_1[H_2O_2](1 + K_5[H^+])}. \qquad (24)$$

Inspection of equation (24) reveals that this product inhibited rate equation does not readily simplify to either first order kinetics at low $[H_2O_2]$ or zero kinetics at high $[H_2O_2]$. The form of the rate equation is further complicated by recognition that the terms $[H_2O_2]$, $[O_2]$ and $[H^+]$ relate to the concentration of these species *at the electrode surface*. Under steady-state conditions, the surface concentration may be related to the bulk concentration, the diffusion layer thickness and the rate at which the species is either being consumed or produced at the overall reaction, by application of Fick's First Law. Thus the surface concentrations of H_2O_2, O_2 and H^+ are given by

$$[H_2O_2] = [H_2O_2]_{bulk} - jk_D\, D_{H_2O_2}^{-2/3}\, \omega^{-1/2}. \qquad (25)$$

$$[O_2] = [O_2]_{bulk} + jk_D\, D_{O_2}^{-2/3}\, \omega^{-1/2}, \qquad (26)$$

$$[H^+] = [H^+]_{bulk} + 2jk_D\, D_{H^+}^{-2/3}\, \omega^{-1/2}, \qquad (27)$$

where k_D is given by

$$k_D = 1.61\, \nu^{1/6}. \qquad (28)$$

$[O_2]_{bulk}$ and $[H^+]_{bulk}$ refer to the bulk concentrations of O_2 and H^+ respectively, and D_{O_2} and D_{H^+} are the diffusion coefficients for these species.

Substitution of the rate- and diffusion-dependent expressions (25)–(28) into the product-inhibited Michaelis–Menten rate equation (24) yields a third-order polynomial in rate in terms of the bulk concentrations of the reactant and products.

$$0 = \alpha j^3 + \beta j^2 + \chi j + \delta \qquad (29)$$

where the polynomial coefficients are given by

$$\alpha = -2K_1K_5k_D^2 D_{H_2O_2}^{-2/3} D_{H^+}^{-2/3}\, \omega^{-1}, \qquad (30)$$

$$\beta = K_4 k_D D_{O_2}^{-2/3}\omega^{-1/2} + 2K_1K_5[H_2O_2]_{bulk}k_D D_{H^+}^{-2/3}\omega^{-1/2} - K_1 k_D D_{H_2O_2}^{-2/3}\omega^{-1/2}(1 + K_5[H^+]_{bulk}), \qquad (31)$$

$$\chi = 1 + K_4[O_2]_{bulk} + k_2 N K_1 k_D D_{H_2O_2}^{-2/3}\omega^{-1/2} + K_1[H_2O_2]_{bulk}(1 + K_5[H^+]_{bulk}), \qquad (32)$$

$$\delta = -k_2 N K_1 [H_2O_2]_{bulk}. \qquad (33)$$

Ascertaining the validity of the mechanism and evaluating the kinetic parameters requires comparison of the roots of this third-order polynomial with the experimental data.

Optimization of parameters for modified Michaelis–Menten mechanism

The three real roots for a third-order polynomial in variable x of the general form

$$0 = x^3 + Ax^2 + Bx + C, \tag{34}$$

where A, B and C are real, can be solved using Viète's method [31] in terms of an angle, ϕ, calculated by

$$\phi = \cos^{-1}\left(\frac{2A^3 - 9AB + 27C}{2(A^2 - 3AB)^{3/2}}\right). \tag{35}$$

The three roots λ_1, λ_2 and λ_3 are given by

$$\lambda_1 = -2\left(\frac{A^2 - 3B}{9}\right)^{1/2} \cos\left(\frac{\phi}{3}\right) - \frac{A}{3}, \tag{36}$$

$$\lambda_2 = -2\left(\frac{A^2 - 3B}{9}\right)^{1/2} \cos\left(\frac{\phi + 2\pi}{3}\right) - \frac{A}{3}, \tag{37}$$

$$\lambda_3 = -2\left(\frac{A^2 - 3B}{9}\right)^{1/2} \cos\left(\frac{\phi + 4\pi}{3}\right) - \frac{A}{3}. \tag{38}$$

The rate equation polynomial given by (29) was transformed into the general form required for Viète's method by division of each of the polynomial coefficients by α.

These operations were encoded in a purpose written computer program [26] incorporating a Simplex [23–25] optimization routine. Inspection of equations (30) to (33) reveals that four mechanistic parameters require optimization; K_1, K_4, K_5 and the product k_2N. Values for D_{O_2} and D_{H^+} were obtained from the literature and taken as 1.93×10^{-9} m^2 s^{-1} [27] and 9.31×10^{-9} m^2 s^{-1} [32] respectively. In light of the range of values for the diffusion coefficient of H_2O_2 obtainable from a series of Koutecky–Levich plots (as shown in Fig. 3), it was thought prudent to optimize this parameter together with the kinetic and binding constant parameters in the Simplex calculation. The Simplex was forced to deal with positive values of the parameters through optimization of the natural logarithm of each parameter.

The Simplex was primed with experimental rates for each concentration and rotation rate shown in Fig. 1 with a constant bulk dissolved oxygen concentration of zero (given that the system was degassed rigorously before and during experimentation) and a bulk hydrogen ion concentration dictated by the electrolyte pH.

Initial optimization studies revealed that only one of the polynomial roots, λ_3, afforded positive real values for j. This significantly simplified the goal-seeking implicit in the Simplex process. The parameters for the data set were optimized on this basis and a minimum in the sum of residuals, r_s, was obtained within 1000 iterations where r_s is given by

$$r_s = \Sigma(j - \lambda_3)^2 \tag{39}$$

Table 2.
Optimised parameters for the product-inhibited Michaelis–Menten mechanism

Parameter	Value
K_1	0.357 m^3 mol^{-1}
k_2N	1.01×10^{-3} mol m^{-2} s^{-1}
K_4	0.149 m^3 mol^{-1}
K_5	0.054 m^3 mol^{-1}
$D_{H_2O_2}$	0.66×10^{-9} m^2 s^{-1}
r_s	5.45×10^{-9} (mol m^{-2} s^{-1})^2
d_{av}	0.127 mA cm^{-2}

for each data point (126 data points in the data set). The average deviation between the observed and calculated current densities, d_{av}, is given by

$$d_{av} = nF\sqrt{\left(\frac{r_s}{126}\right)}. \tag{40}$$

The optimized parameters are listed in Table 2 and synthetic i vs $[H_2O_2]_{bulk}$ curves based on these values and transformed from rate using (13) are shown together with the experimental data in Fig. 1.

The synthetic response curves are in good agreement with the experimental data with small d_{av} (0.8% of maximum current density) and exhibiting no systematic deviations for any rotation rate or H_2O_2 concentration. Replicate sets of experimental data show equally good fits with small differences in the optimised parameters consummate with the expected variation in active surface area of the electrode.

The mechanism we report here is extremely sensitive to the diffusion coefficient, with the sum of residuals exhibiting a sharp minimum for the optimised value. This value is somewhat lower than those reported predominantly in the literature [19,27,28,33], a summary of which is presented in Table 3. In this study we find an optimal value of $D_{H_2O_2}$ to be 0.66×10^{-9} m^2 s^{-1} whereas interpolation of the data presented in Table 3 would suggest a value approximately twice this at 20°C. The methods used by these previous workers rely upon the assumption that the electrochemical reaction with H_2O_2 (either oxidation or reduction) is taking place under conditions where the reaction is entirely diffusion limited. We have shown in this work for oxidation of H_2O_2 at platinum that this assumption is inappropriate and consequently affords misleading values for $D_{H_2O_2}$ from Koutecky–Levich plots. This is demonstrated in Fig. 3 where, depending on H_2O_2 concentration, $D_{H_2O_2}$ can be found in the range $0.6–1.4 \times 10^{-9}$ m^2 s^{-1}. These effects may be accounted for by inspection of the calculated surface concentration data for H_2O_2, H^+ and O_2 in Fig. 5 as a function of bulk $[H_2O_2]$ based upon equations (25) to (28) and the optimised rate parameters (for the lowest rotation rate explored). It is clear that the surface concentration of H_2O_2 only approaches zero

Table 3.
Reported values for the diffusion coefficient of hydrogen peroxide

Workers	$D_{H_2O_2} \times 10^9$ ($m^2\ s^{-1}$)	T (°C)	Method
van Stroe-Biezen *et al*. [27]	1.43	25	Koutecky–Levich
van Stroe-Biezen *et al*. [27]	1.83	37	Koutecky–Levich
Brestovisky *et al*. [33]	1.2	Not stated	Reverse Pulse Polarography
Prabhu *et al*. [19]	1.21–1.61	25	Chronoamperometry
Prabhu *et al*. [19]	1.07–1.56	25	Chronopotentiometry
Borggaard [28]	0.88	10	Polarography
Borggaard [28]	1.35	20	Polarography
Borggaard [28]	1.75	30	Polarography
Borggaard [28]	2.20	40	Polarography
This work	0.66	20	Michaelis–Menten kinetics

(and hence overall diffusion control) at low bulk concentrations; above 20 mM the surface concentration increases linearly and adopts a value some 18 mM below that of the bulk. Furthermore, we calculate that at the highest rotation rate explored a completely linear dependence between surface and bulk concentration develops at all concentrations.

Honda *et al*. [34] have used a value for $D_{H_2O_2}$ of $0.5 \times 10^{-9}\ m^2\ s^{-1}$ which is similar to that found here and is ascribed to a report by Littauer and Tsai [35] for studies of H_2O_2 in alkaline solutions. Inspection of the article by Littauer and Tsai [35], however, reveals this value was interpreted as being appropriate for the perhydroxy ion rather than H_2O_2 and cannot be taken as supporting evidence for our result.

Whilst we report a single new value for $D_{H_2O_2}$ that accounts for both surface reaction kinetics and non-diffusion limited conditions, validation of this new value is required through some independent means.

Figures 6 and 7 display the calculated fractional coverages for each surface species in this mechanism as a function of bulk H_2O_2 concentration at the highest and lowest rotation rates respectively. At all rotation rates the fractional coverage of the binding site, $Pt(OH)_2$, decreases rapidly with increasing $[H_2O_2]$ with a concomitant increase in coverage of the $Pt(OH)_2{\cdot}H_2O_2$ complex. This increase continues until a plateau is achieved which corresponds to the maximum observed reaction rate according to equations (16) and (22). The coverage at the plateau

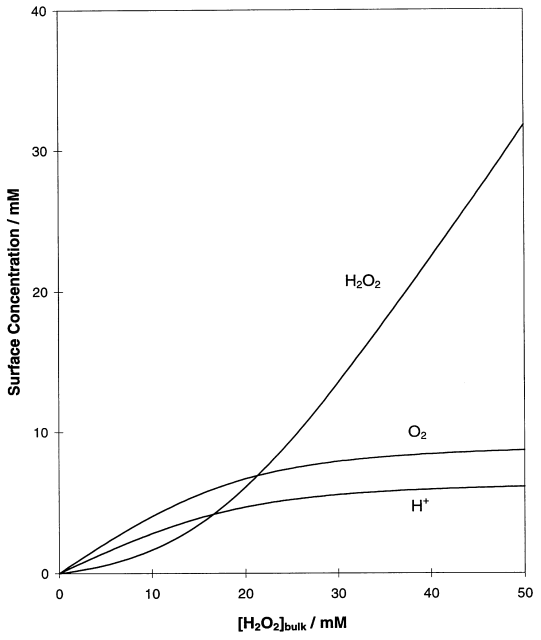

Fig. 5. Calculated surface concentrations for H_2O_2, O_2 and H^+ as a function of $[H_2O_2]_{bulk}$ based on the optimized model parameters for a rotation rate of 630 r.p.m.

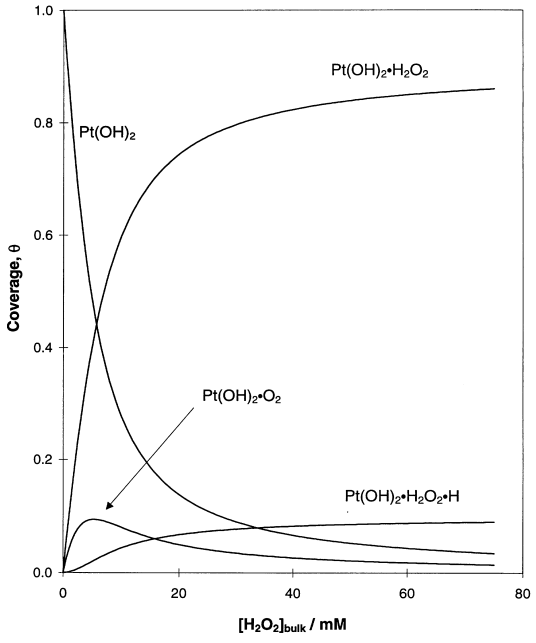

Fig. 6. Calculated surface coverages of all surface species involved in the mechanism as a function of $[H_2O_2]_{bulk}$ based on the optimised model parameters for a rotation rate of 10,000 r.p.m.

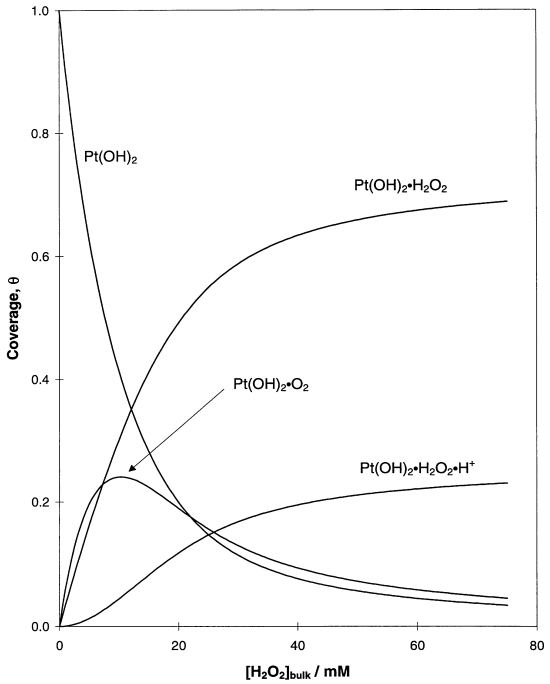

Fig. 7. Calculated surface coverages of all surface species involved in the mechanism as a function of $[H_2O_2]_{bulk}$ based on the optimised model parameters for a rotation rate of 630 r.p.m.

is determined by the extent of inhibition at each rotation rate. The two inhibiting reactions prevail over two separate concentration regions.

Dioxygen inhibition forms a transient surface species at low concentrations through complexation with the binding site in competition with H_2O_2. This is particularly pronounced at low rotation rates where there is a greater surface concentration of O_2 than at higher rotation rates. This inhibition is the predominant cause for the dependence on ω for the linear response at low $[H_2O_2]$ as shown in Fig. 1. The ratio of the binding constants for H_2O_2 and O_2, K_1/K_4, is such that surface complexation of H_2O_2 is favoured. Consequently, a maximum for surface coverage by O_2 inhibition is evident as $[H_2O_2]$ is increased, the maxima having greatest values at low rotation rates as shown in Figs 6 and 7. This behaviour accounts for the pronounced deviation at low rotation rates and low $[H_2O_2]$ in the series of Hane's plots shown in Fig. 4.

Inhibition by protonation of the $Pt(OH)_2{\cdot}H_2O_2$ complex follows the development of this species due to the requirement for prior formation of the complex and the consummate increase in surface concentration of H^+ with increasing oxidation rate. Thus, a plateau in surface coverage of the protonated $Pt(OH)_2{\cdot}H_2O_2$ complex is evident with greatest coverage at low rotation rates.

An operational value for K_M may be evaluated for each rotation rate. This parameter (defined as the concentration for half coverage by the $Pt(OH)_2{\cdot}H_2O_2$ complex) does not directly relate to the binding constant K_1 due to the combination of the two inhibiting equilibria. Consequently, inspection of Figs 6 and 7 reveals that K_M has a value of 20.5 mM at 630 r.p.m. decreasing to 7.1 mM at 10,000 r.p.m. The latter value approaches the theoretical value of 2.8 mM given by the inverse of K_1 for an infinitely high rotation rate where the two inhibiting reactions would be absent.

The mechanism proposed in this article for the oxidation of H_2O_2 at Pt demonstrates the need for controlling the mass-transport conditions for this reaction. Whilst we propose a mechanism based on interpretation of experimental data collected over a wide range of $[H_2O_2]$ and rotation rates, there is no reason to expect this not to follow at the low concentrations likely to be encountered in biosensors. Maximum electrode response and sensitivity can only be obtained under conditions where the products are rapidly removed from the vicinity of the electrode. This model will be applied to an examination of the kinetics for H_2O_2 oxidation at metallized carbon powders.

ACKNOWLEDGEMENTS

The authors wish to acknowledge the Massey University Research and Research Equipment Fund (MURF and MUREF 1996) for contributions to the funding of this work.

REFERENCES

1. L. C. Clark, US Patent 3534955 (1970).
2. H. P. Bennetto, D. R. DeKeyser, G. M. Delaney, A. Koshy, J. R. Mason, G. Mourla, L. A. Razack, J. L. Sterling, C. F. Thurston, D. G. Anderson and W. H. Mullen, *Int. Ind. Biotechnol.* **8,** 5 (1985).
3. S. F. White, A. P. F. Turner, U. Bilitewski, R. D. Schmid and J. Bradley, *Electroanalysis* **6,** 625 (1994).
4. S. Mukerjee, *J. Appl. Electrochem.* **20,** 537 (1990).
5. J. Wang, M. Pedrero, P. V. A. Pamidi and X. Cai, *Electroanalysis* **7,** 1032 (1995).
6. W. A. Collier, D. Janssen and A. L. Hart, *Biosens. Bioelectron.* **11,** 1041 (1996).
7. P. N. Bartlett and K. F. E. Pratt, *Biosens. Bioelectron.* **8,** 451 (1993).
8. Y. Zhang and G. S. Wilson, *J. Electroanal. Chem.* **345,** 253 (1993).
9. A. J. Bard and L. R. Faulkner, *Electrochemical Methods, Fundamentals and Applications*, p. 291, Wiley, New York (1980).
10. H. B. Urbach and R. J. Bowen, *Electrochim. Acta* **14,** 927 (1969).
11. J. J. Lingane, *J. Electroanal. Chem.* **2,** 296 (1961).
12. J. J. Lingane and P. J. Lingane, *J. Electroanal. Chem.* **5,** 411 (1963).
13. L. Miller, *J. Electroanal. Chem.* **16,** 531 (1968).
14. F. C. Anson and J. J. Lingane, *J. Am. Chem. Soc.* **79,** 4901 (1957).
15. A. Hickling and W. Wilson, *J. Electrochem. Soc.* **98,** 425 (1951).
16. Y. L. Sandler and D. A. Pantier, *J. Electrochem. Soc.* **112,** 928 (1965).

17. L. Gorton, *Anal*. *Chim*. *Acta* **178,** 247 (1985).
18. D. A. Johnston, M. F. Cardosi and D. H. Vaughan, *Electroanalysis* **7,** 520 (1995).
19. V. G. Prabhu, L. R. Zarapkar and R. G. Dhaneshwar, *Electrochim*. *Acta* **26,** 725 (1981).
20. W. H. Mullen, S. J. Churchouse, F. H. Keedy and P. M. Vadgama, *Clin*. *Chem*. *Acta* **157,** 191 (1986).
21. M. Mascini and G. Palleschi, *Selective Electrode Rev*. **11,** 191 (1989).
22. G. E. P. Box and K. B. Wilson, *J*. *Roy*. *Statist*. *Soc*., *Ser*. *B* **13,** 1 (1951).
23. W. Spendley, G. R. Hext and F. R. Himsworth, *Technometrics* **4,** 441 (1962).
24. J. A. Nedler and R. Mead, *Computer J*. **7,** 308 (1965).
25. L. A. Yarbro and S. N. Deming, *Anal*. *Chim*. *Acta* **73,** 391 (1974).
26. Modified version of code written by A. Kucernak, Department of Chemistry, Imperial College of Science, Technology and Medicine, London, UK (1986).
27. S. A. M. van Stroe-Biezen, F. M. Everaerts, L. J. J. Janssen and R. A. Tacken, *Anal*. *Chim*. *Acta* **273,** 553 (1993).
28. O. K. Borggaard, *Acta Chem*. *Scand*. **26,** 3393 (1972).
29. C. S. Hanes, *Biochem*. *J*. **26,** 1406 (1932).
30. H. Lineweaver and D. Burk, *J*. *Am*. *Chem*. *Soc*. **56,** 658 (1934).
31. First appears in Francois Viète's treatise *De emendatione* published 1615. Quoted by W. H. Press, B. P. Flannery, S. A. Teulosky and W. T. Vetterling, *Numerical Recipes in Pascal*, p. 164, Cambridge University Press, Cambridge (1989).
32. P. W. Atkins, *Physical Chemistry*, p. 836 Oxford University Press, Oxford (1978).
33. A. Brestovisky, E. Kirowa-Eisner and J. Osteryoung, *Anal*. *Chem*. **55,** 2063 (1983).
34. M. Honda, T. Kodera and H. Kita, *Electrochim*. *Acta* **28,** 727 (1983).
35. E. L. Littauer and K. C. Tsai, *Electrochim*. *Acta* **24,** 681 (1979).